On the Eigenvalue Tracking of Large-Scale Systems

Andreas Bouterakos[a], Joseph McKeon[a] Georgios Tzounas[a*]

School of Electrical and Electronic Engineering, University College Dublin, Ireland

*Corresponding author.

E-mail address: georgios.tzounas@ucd.ie

Abstract The paper focuses on the problem of tracking eigenvalue trajectories in large-scale power system models as system parameters vary. A continuation-based formulation is presented for tracing any single eigenvalue of interest, which supports sparse matrix representations and accommodates both explicit and semi-implicit differential-algebraic models. Key implementation aspects, such as numerical integration, matrix updates, derivative approximations, and handling defective eigenvalues, are discussed in detail and practical recommendations are duly provided. The tracking approach is demonstrated through a comprehensive case study on the IEEE 39-bus system, as well as on a realistic dynamic model of the Irish transmission system.

Keywords: Small-signal stability analysis (SSSA), eigenvalue tracking, continuation methods, large-scale systems, frequency regulation (FR) mode.

1   Introduction

1.1   Motivation

Eigenvalue analysis is a fundamental component of power system stability assessment. It is widely used to evaluate the system's small-signal stability margin and to characterize the structure of its dynamic modes [1]. Within this framework, eigenvalue tracking – the process of monitoring how eigenvalue trajectories evolve with variation of system parameters – is a key task. In real-world power system models, eigenvalue tracking typically involves large, non-symmetric matrices/pencils and can be a computationally intensive and numerically challenging problem.

1.2   Literature Review

The most straightforward approach to eigenvalue tracking is to perform a full eigendecomposition of the system's state matrix or pencil at each parameter value of interest. Since standard eigensolvers commonly reorder eigenvalues between computations, this approach must be combined with a technique to sort eigenvalues consistently at successive parameter values. A simple approach is to pair eigenvalues based on Euclidean distances in the complex plane; however, this often leads to erroneous results, especially when different eigenvalues come close together or cross. More robust approaches include using metrics based on eigenvectors, such as participation factors [2] or modal assurance criteria [3].

Repeated eigendecomposition starts to perform poorly as the system size increases. This is because QR and QZ factorizations – the standard dense-matrix methods for computing the full spectrum of general non-symmetric eigenvalue problems – have computational complexity and memory requirements that scale cubically with size [4]. In practice, for large power system models involving thousands to tens of thousands of variables, computing eigenvalue trajectories becomes prohibitively expensive. To address this, alternative solvers designed for large sparse matrices can be employed, such as Krylov-based or contour integration methods [5–7]. These are subspace methods which restrict the computation to only a part of the spectrum. This is generally not a limitation for eigenvalue tracking, as in practice only the trajectories of a single or a few modes, conventionally the most critical ones for stability, are of interest. However, the main difficulty in this case lies in the need for a proper spectral transformation (such as Cayley or shift & invert) that can effectively target a region of the complex plane containing the eigenvalue of interest [1]. These transformations require careful tuning at each parameter value, and maintaining consistency across a range in a reliable and automatic manner can be impractical.

An alternative approach to eigenvalue tracking is offered by the family of continuation-based methods. The idea of continuation is to trace the solution of a problem that depends on a varying parameter, by incrementally updating it through a numerical method using previous values. These types of techniques have been applied with great success in power system applications; for instance, they have been widely used to trace equilibria in long-term voltage stability studies [8,9]. In the context of eigenvalue tracking, existing works explore continuation-based methods to follow the trajectory of either a single eigenpair at a time [10, 11] or of multiple eigenpairs simultaneously [12, 13]. The focus in these studies is on critical synchronous machine electromechanical modes.

Despite these advances, the use of continuation-based eigenvalue tracking techniques remains limited. For small to medium-sized systems, repeated eigendecomposition is typically preferred due to its simplicity and reasonable efficiency. For large systems, eigenvalue tracking is most often completely avoided. The key reason lies in how existing formulations handle differential-algebraic models: they rely on dense matrix computations, which do not scale well thus preventing these methods from realizing what, to the authors' view, could be their main competitive advantage, namely, the ability to offer significant computational speedups in large-scale settings. An additional reason is that several important implementation aspects, such as parameter step size selection, handling of defective eigenvalues [14–16], matrix updates, and derivative calculations, have not been sufficiently addressed.

1.3 Contributions

The contributions of this paper are as follows:

- A general continuation-based tracking formulation is developed that supports both dense and sparse matrix representations, and is compatible with both explicit and semi-implicit differential-algebraic

2

forms of power system models.

- Practical and critical implementation aspects – such as multiple eigenpair tracking, parameter step size selection, defective eigenvalue handling, matrix updates, and derivative estimations, – are addressed in detail.

These contributions are supported by a comprehensive case study. First, continuation-based tracking is applied to the frequency regulation (FR) mode, a dynamic mode that plays an increasingly important role in analyzing system-wide oscillatory behaviors introduced by frequency control loops. Second, it is benchmarked against repeated eigendecomposition on a large-scale model of the all-island Irish transmission system, with emphasis on computational cost and scalability.

1.4   Paper Organization

The remainder of the paper is structured as follows. Section 2 provides preliminaries on small-signal stability analysis (SSSA). The formulation and implementation aspects of the eigenvalue tracking approach adopted are discussed in Section 3. Section 4 presents simulation results on the tracking of FR modes, based on the IEEE 39-bus system, as well as on a real-world size model of the Irish transmission system. Finally, conclusions are drawn and future work directions are outlined in Section 5.

2   Small-Signal Stability Analysis

2.1   Power System Model

In short-term stability analysis, power system dynamics can be studied through a set of non-linear, *semi-implicit* differential algebraic equations (DAEs), as follows [17]:

$$
\begin{bmatrix} \boldsymbol{T} & \boldsymbol{0}_{n,m} \\ \boldsymbol{R} & \boldsymbol{0}_{m,m} \end{bmatrix} \begin{bmatrix} \boldsymbol{x}'(t) \\ \boldsymbol{y}'(t) \end{bmatrix} = \begin{bmatrix} \boldsymbol{f}(\boldsymbol{x}(t), \boldsymbol{y}(t)) \\ \boldsymbol{g}(\boldsymbol{x}(t), \boldsymbol{y}(t)) \end{bmatrix} \tag{1}
$$

where $\boldsymbol{x}(t) : [0, \infty) \to \mathbb{R}^n$ are the state variables of dynamic components connected to the power network (generators, dynamic loads, automatic controls, etc.); $\boldsymbol{y}(t) : [0, \infty) \to \mathbb{R}^m$ are the algebraic variables (bus voltages and power injections, auxiliary variables that define control setpoints, etc.); $\boldsymbol{f} : \mathbb{R}^{n+m} \to \mathbb{R}^n$ and $\boldsymbol{g} : \mathbb{R}^{n+m} \to \mathbb{R}^m$ are functions that define, respectively, the differential and algebraic equations; $\boldsymbol{T} \in \mathbb{R}^{n \times n}$, $\boldsymbol{R} \in \mathbb{R}^{m \times n}$; and $\boldsymbol{0}_{n,m}$ denotes the zero matrix of dimensions $n \times m$. Note that (1) preserves the separation between differential and algebraic variables, consistent with DAE theory: algebraic variables may vary in time but are not governed by differential equations and, by definition, do not have nonzero finite time constants [18]. The semi-implicit DAE form (1) is a generalization of the conventional, *explicit*

DAE form [19]:

$$x'(t) = f(x(t), y(t))$$
$$0_{m,1} = g(x(t), y(t)) \tag{2}$$

In the remainder of the paper we work with (1), which offers certain practical advantages over (2), such as increased sparsity and convenient switching of states to algebraic variables. The explicit form can be always retrieved as a special case, for $T = I_n$, $R = 0_{m,n}$, where I_n is the $n \times n$ identity matrix.

2.2 Eigenvalue Analysis

We are interested in studying the system's behavior in response to the variation of certain system parameters. To this end, the parameters of interest are expressed as functions of a scalar continuation parameter $p \in \mathbb{R}$ and (1) is rewritten as follows:

$$\begin{bmatrix} T(p) & 0_{n,m} \\ R(p) & 0_{m,m} \end{bmatrix} \begin{bmatrix} x' \\ y' \end{bmatrix} = \begin{bmatrix} f(x, y, p) \\ g(x, y, p) \end{bmatrix} \tag{3}$$

where the dependency of time is omitted for simplicity. Considering small disturbances, and aiming at using well-established results from linear stability theory, (3) can be linearized around an equilibrium $(x_o, y_o) := [x_o^\mathsf{T}, y_o^\mathsf{T}]^\mathsf{T}$ (T indicating the transpose) as follows:

$$\begin{bmatrix} T(p) & 0_{n,m} \\ R(p) & 0_{m,m} \end{bmatrix} \begin{bmatrix} \Delta x' \\ \Delta y' \end{bmatrix} = \begin{bmatrix} f_x(p) & f_y(p) \\ g_x(p) & g_y(p) \end{bmatrix} \begin{bmatrix} \Delta x \\ \Delta y \end{bmatrix} \tag{4}$$

where $\Delta x = x - x_o$, $\Delta y = y - y_o$; f_x, f_y, g_x, g_y are the Jacobian matrices evaluated at (x_o, y_o), for example, $f_x = \partial f / \partial x |_{(x_o, y_o)}$. System (4) is of the form:

$$\mathbf{E}(p)\,\mathbf{x}' = \mathbf{A}(p)\,\mathbf{x} \tag{5}$$

where $\mathbf{x} = (\Delta x, \Delta y)$ and

$$\mathbf{E}(p) \equiv \begin{bmatrix} T(p) & 0_{n,m} \\ R(p) & 0_{m,m} \end{bmatrix}, \quad \mathbf{A}(p) \equiv \begin{bmatrix} f_x(p) & f_y(p) \\ g_x(p) & g_y(p) \end{bmatrix} \tag{6}$$

Alternatively to working directly with (4), algebraic variables can be eliminated from the linearized system, leading to:

$$\Delta x' = [T^{-1}(p) \cdot (f_x(p) - f_y(p) \cdot (g_y(p) - R(p)T^{-1}(p)f_y(p))^{-1} \cdot (g_x(p) - R(p)T^{-1}(p)f_x(p)))]\Delta x \tag{7}$$

which is in the form of (5), where in this case $\mathbf{x} \equiv \Delta \boldsymbol{x}$ and

$$\mathbf{E}(p) \equiv \boldsymbol{I}_n,$$

$$\mathbf{A}(p) \equiv \boldsymbol{T}^{-1}(p) \cdot (\boldsymbol{f}_x(p) - \boldsymbol{f}_y(p) \cdot (\boldsymbol{g}_y(p) - \boldsymbol{R}(p)\boldsymbol{T}^{-1}(p)\boldsymbol{f}_y(p))^{-1} \cdot (\boldsymbol{g}_x(p) - \boldsymbol{R}(p)\boldsymbol{T}^{-1}(p)\boldsymbol{f}_x(p))) \tag{8}$$

Systems (4) and (7) are dynamically equivalent, in the sense that they have the same n finite eigenvalues. Yet, (4) has additionally the infinite eigenvalue $s \to \infty$, with algebraic multiplicity m, see [20]. Moreover, the matrices that define (4) are sparse, whereas the state matrix in (7) is dense, which is an important difference when it comes to numerical computations [4]. In particular, for small systems, (7) is preferred and the full set of its finite eigenvalues problem can be obtained efficiently, typically through QR factorization. On the other hand, (4) is preferable for large systems. A subset of the eigenvalues in this case can be found with appropriate sparse algorithms [4].

Derivations in this paper are provided considering the general system form (5). Their specific expressions for (4) and (7) can be then obtained as special cases in a straightforward way, i.e., by substituting the expressions of $\mathbf{E}(p)$ and $\mathbf{A}(p)$ from (6), (8), respectively. That said, we proceed to apply the Laplace transform to (5):

$$[s(p)\mathbf{E}(p) - \mathbf{A}(p)]\,\mathcal{L}\{\mathbf{x}\} = \mathbf{E}(p)\mathbf{x}(0) \tag{9}$$

where $s(p)$ is a complex frequency in the S-plane. The polynomial matrix

$$\mathbf{P}(s, p) = s(p)\mathbf{E}(p) - \mathbf{A}(p) \tag{10}$$

is important in the study of (5) and is called the system's *matrix pencil* [1,21]. In particular, every value of s that when substituted to (10) leads to a singular $\mathbf{P}(s, p)$ is an eigenvalue of (5), with the associated algebraic problem being:

$$\mathbf{P}(s, p)\,\boldsymbol{\phi}(p) = \mathbf{0}_{r,1} \tag{11}$$

$$\boldsymbol{\psi}(p)\,\mathbf{P}(s, p) = \mathbf{0}_{1,r} \tag{12}$$

where every non-trivial vector $\boldsymbol{\phi}(p)$ satisfying (11) is a right eigenvector; and every non-trivial vector $\boldsymbol{\psi}(p)$ satisfying (12) is a left eigenvector. The dimensions of $\mathbf{P}(s, p)$ are $r \times r$, where the value of r depends on whether $\mathbf{E}$, $\mathbf{A}$ are defined from (6), in which case $r = n$, or (8), in which case $r = n + m$.

3   Eigenvalue Tracking

In this section, we describe the approach adopted to track targeted solutions of (11) as the continuation parameter p varies. We first focus on the tracking of a single eigenvalue and then address the problem

of tracking multiple eigenvalues.

3.1 Tracking a Single Eigenpair

We start by differentiating (11) with respect to p:

$$\dot{\mathbf{P}}(s,p)\,\boldsymbol{\phi}(p) + \mathbf{P}(s,p)\,\dot{\boldsymbol{\phi}}(p) = \mathbf{0}_{r,1} \tag{13}$$

where:

$$\dot{\mathbf{P}}(s,p) = \dot{s}(p)\mathbf{E}(p) + s(p)\dot{\mathbf{E}}(p) - \dot{\mathbf{A}}(p) \tag{14}$$

and $\dot{s} = \partial s/\partial p$, $\dot{\boldsymbol{\phi}} = \partial \boldsymbol{\phi}/\partial p$, $\dot{\mathbf{E}} = \partial \mathbf{E}/\partial p$, $\dot{\mathbf{A}} = \partial \mathbf{A}/\partial p$.

Equation (13) can be equivalently written as:

$$\mathbf{E}\boldsymbol{\phi}\dot{s} + [s\mathbf{E} - \mathbf{A}]\dot{\boldsymbol{\phi}} = -[s\dot{\mathbf{E}} - \dot{\mathbf{A}}]\boldsymbol{\phi} \tag{15}$$

where the dependency on p is omitted for simplicity. The dynamical system (15), which describes the evolution a single eigenpair with respect to the parameter p, consists of r equations and $r+1$ unknowns, namely s and $\boldsymbol{\phi}$. To make this system well-posed, we additionally impose the following eigenvector normalization condition:

$$\boldsymbol{\phi}^{\mathsf{T}}\mathbf{E}\boldsymbol{\phi} = c \tag{16}$$

where c is a constant, e.g., $c = 1$. Differentiation of (16) gives:

$$2\boldsymbol{\phi}^{\mathsf{T}}\mathbf{E}\dot{\boldsymbol{\phi}} = -\boldsymbol{\phi}^{\mathsf{T}}\dot{\mathbf{E}}\boldsymbol{\phi} \tag{17}$$

The derivation of (17) is given in the Appendix.

Combining (15), (17):

$$\begin{bmatrix} s\mathbf{E} - \mathbf{A} & \mathbf{E}\boldsymbol{\phi} \\ 2\boldsymbol{\phi}^{\mathsf{T}}\mathbf{E} & 0 \end{bmatrix} \begin{bmatrix} \dot{\boldsymbol{\phi}} \\ \dot{s} \end{bmatrix} = \begin{bmatrix} -(s\dot{\mathbf{E}} - \dot{\mathbf{A}})\boldsymbol{\phi} \\ -\boldsymbol{\phi}^{\mathsf{T}}\dot{\mathbf{E}}\boldsymbol{\phi} \end{bmatrix} \tag{18}$$

Splitting real and imaginary parts, i.e., $\boldsymbol{\phi} = \boldsymbol{\phi}_{\mathrm{r}} + \jmath\boldsymbol{\phi}_{\mathrm{i}}$, $s = s_{\mathrm{r}} + \jmath s_{\mathrm{i}}$, we arrive to the following expression:

$$\mathbf{M}(\mathbf{y})\,\dot{\mathbf{y}} = \boldsymbol{h}(\mathbf{y}) \tag{19}$$

where $\mathbf{y} = \mathbf{y}(p) = (\phi_{\mathrm{r}}, \phi_{\mathrm{i}}, s_{\mathrm{r}}, s_{\mathrm{i}})$, with $\mathbf{y} \in \mathbb{R}^{2r+2}$; and:

$$
\mathbf{M}(\mathbf{y}) = \begin{bmatrix} s_{\mathrm{r}}\mathbf{E} - \mathbf{A} & -s_{\mathrm{i}}\mathbf{E} & \mathbf{E}\phi_{\mathrm{r}} & -\mathbf{E}\phi_{\mathrm{i}} \\ s_{\mathrm{i}}\mathbf{E} & s_{\mathrm{r}}\mathbf{E} - \mathbf{A} & \mathbf{E}\phi_{\mathrm{i}} & \mathbf{E}\phi_{\mathrm{r}} \\ 2\phi_{\mathrm{r}}^{\mathsf{T}}\mathbf{E} & -2\phi_{\mathrm{i}}^{\mathsf{T}}\mathbf{E} & 0 & 0 \\ 2\phi_{\mathrm{i}}^{\mathsf{T}}\mathbf{E} & 2\phi_{\mathrm{r}}^{\mathsf{T}}\mathbf{E} & 0 & 0 \end{bmatrix}
$$

$$
\boldsymbol{h}(\mathbf{y}) = \begin{bmatrix} \dot{\mathbf{A}}\phi_{\mathrm{r}} - s_{\mathrm{r}}\dot{\mathbf{E}}\phi_{\mathrm{r}} + s_{\mathrm{i}}\dot{\mathbf{E}}\phi_{\mathrm{i}} \\ \dot{\mathbf{A}}\phi_{\mathrm{i}} - s_{\mathrm{i}}\dot{\mathbf{E}}\phi_{\mathrm{r}} - s_{\mathrm{r}}\dot{\mathbf{E}}\phi_{\mathrm{i}} \\ -\phi_{\mathrm{r}}^{\mathsf{T}}\dot{\mathbf{E}}\phi_{\mathrm{r}} + \phi_{\mathrm{i}}^{\mathsf{T}}\dot{\mathbf{E}}\phi_{\mathrm{i}} \\ -\phi_{\mathrm{r}}^{\mathsf{T}}\dot{\mathbf{E}}\phi_{\mathrm{i}} - \phi_{\mathrm{i}}^{\mathsf{T}}\dot{\mathbf{E}}\phi_{\mathrm{r}} \end{bmatrix}
$$

(19) is a set of differential equations with state-dependent mass matrix $\mathbf{M}(\mathbf{y})$. Note that (17) is used instead of (16) because directly imposing the normalization as an algebraic constraint would result in a singular matrix $\mathbf{M}(\mathbf{y})$.

Tracking is performed by numerically integrating (19) over a parameter range or interest $[p_{init}, p_{fin}]$. Given p_{init}, the corresponding initial condition $\mathbf{y}(p_{init})$ for the state vector $\mathbf{y}$ is obtained by solving once the eigenvalue problem (11). In all subsequent steps, only the power flow problem is solved to update the operating point and reconstruct the matrices $\mathbf{A}(p)$ and $\mathbf{E}(p)$. The matrix derivatives $\dot{\mathbf{E}}$ and $\dot{\mathbf{A}}$ in this paper are calculated numerically using first-order finite differences.

The integration proceeds iteratively until $p = p_{fin}$, as follows:

1. Given a step size Δp, the parameter is updated as $p_{k+1} = p_k + \Delta p$.

2. The mass matrix $\mathbf{M}(\mathbf{y}_k)$ and right-hand side $\boldsymbol{h}(\mathbf{y}_k)$ are evaluated, and the state vector is updated using the chosen integration method. For example, using the forward Euler method yields:

$$
\mathbf{y}_{k+1} = \mathbf{y}_k + \Delta p\, \mathbf{M}^{-1}(\mathbf{y}_k)\, \boldsymbol{h}(\mathbf{y}_k) \tag{20}
$$

The product $\mathbf{M}^{-1}(\mathbf{y}_k)\, \boldsymbol{h}(\mathbf{y}_k)$ can be determined through *LU decomposition* of $\mathbf{M}(\mathbf{y}_k)$.

We note that, like any numerical integration-based scheme, the above process introduces a discretization error, which can be controlled by adapting the step size. Moreover, the error can be effectively eliminated through the addition of a corrector step (e.g., using Newton's method), at an additional computational cost. This is further discussed in Section 4.

3.2 Tracking Multiple Eigenpairs

We extend the above approach to the case of multiple eigenvalues. Let $\boldsymbol{\Phi} \in \mathbb{C}^{r \times \kappa}$ be the matrix whose columns are linearly independent right eigenvectors of κ finite eigenvalues of (10), i.e., $\boldsymbol{\Phi} = [\phi_1\, \phi_2\, \dots\, \phi_\kappa]$,

where $1 \leq \kappa \leq n$. Then, (11) can be generalized as:

$$\mathbf{A}(p)\mathbf{\Phi}(p) - \mathbf{E}(p)\mathbf{\Phi}(p)\mathbf{\Lambda}(p) = \mathbf{0}_{r,\kappa} \tag{21}$$

where $\mathbf{\Lambda}$ is diagonal matrix containing the κ finite eigenvalues of interest. Differentiation with respect to the continuation parameter p gives:

$$\mathbf{A}\dot{\mathbf{\Phi}} + \dot{\mathbf{A}}\mathbf{\Phi} - \dot{\mathbf{E}}\mathbf{\Phi}\mathbf{\Lambda} - \mathbf{E}\dot{\mathbf{\Phi}}\mathbf{\Lambda} - \mathbf{E}\mathbf{\Phi}\dot{\mathbf{\Lambda}} = \mathbf{0}_{r,\kappa} \tag{22}$$

or, equivalently:

$$\begin{bmatrix} \mathbf{A} & -\mathbf{E}\mathbf{\Phi} \end{bmatrix} \begin{bmatrix} \dot{\mathbf{\Phi}} \\ \dot{\mathbf{\Lambda}} \end{bmatrix} - \begin{bmatrix} \mathbf{E} & \mathbf{0} \end{bmatrix} \begin{bmatrix} \dot{\mathbf{\Phi}} \\ \dot{\mathbf{\Lambda}} \end{bmatrix} \mathbf{\Lambda} = \dot{\mathbf{E}}\mathbf{\Phi}\mathbf{\Lambda} - \dot{\mathbf{A}}\mathbf{\Phi} \tag{23}$$

Similar to (15), suitable normalization constraints can be introduced to make (23) well posed. In the multiple-eigenpair case, this leads to a generalized Sylvester equation of the form:

$$\boldsymbol{MX} + \boldsymbol{GXN} = \boldsymbol{F} \tag{24}$$

where $\boldsymbol{X} = (\mathbf{\Phi}, \mathbf{\Lambda})$. To the best of our knowledge, efficient solvers for the numerical solution of (24) in its general form are not available. In the special case where $\boldsymbol{G}$ is the identity matrix, the Bartels-Stewart algorithm can be used, see [22–25]. However, the algorithm does not scale well with system size and thus appears impractical for large-scale power system models. Given these limitations, in this paper we track multiple eigenvalues by applying the single-eigenpair formulation (19) separately to each mode of interest. The tracking process is repeated independently for every eigenpair and is therefore naturally parallelizable.

4   Case Study

This section presents simulation results on the eigenvalue tracking approach described in Section 3. The results in Sections 4.1 and 4.2 are based on the IEEE 39-bus system, detailed data of which can be found in [26]. Then, Section 4.3 considers a real-world size dynamic model of the All-Island Irish Transmission System (AIITS). In all cases, eigenvalue trajectories are compared against those computed via repeated, dense QR factorizations, which serve as the reference. All simulations are carried out with the power system software tool Dome [27]. The version of the software employed in this paper relies on LAPACK 3.10.0 for QR factorization and KLU 5.10.1 for LU factorization.

4.1 IEEE 39-Bus System

The results of this section are based on the IEEE 39-bus system (see Fig. 1). The system comprises 10 synchronous machines (SMs), represented by fourth-order models. Machines are equipped with automatic voltage regulators, power system stabilizers, and turbine governors (TGs). For the purposes of this study, the original system has been modified to reduce by a factor of ten the inertia constant of the SM connected to bus 39.
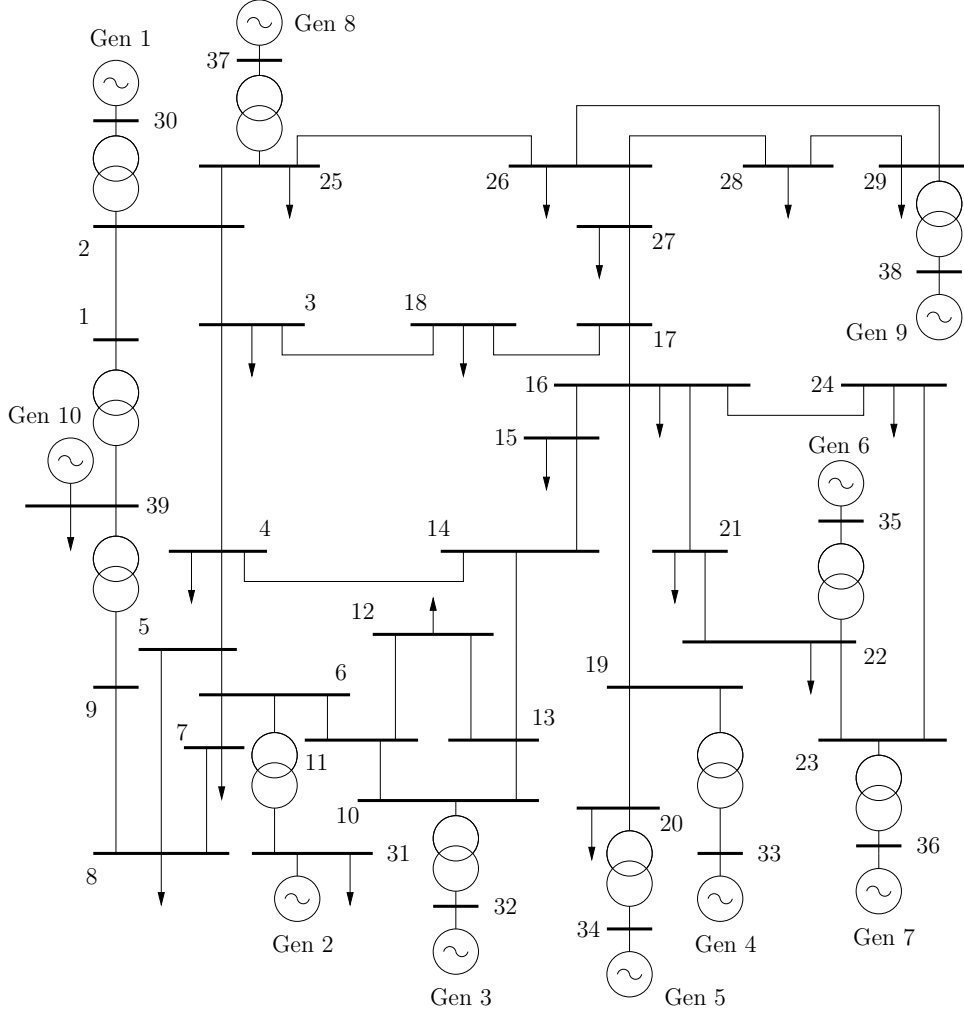

Figure 1: 39-bus system: single-line diagram.

We focus on tracking the system's frequency regulation (FR) mode. This mode emerges with the inclusion of frequency controllers in the system and reflects a coherent response to frequency deviations across the network. Due to its global coherence and the relatively slow response of conventional turbine governors, this mode has also been referred to in the literature as the *common low-frequency mode*. FR modes have drawn interest due to their relevance in understanding potential oscillatory behaviors associated with closed-loop frequency control dynamics, see [28–30]. At the base case operating point of the examined system, the FR mode is represented by the complex pair of eigenvalues $-0.03533 \pm j0.07357$, which has natural frequency 0.01 Hz and damping ratio 43.3%. As shown in Fig. 2a, the

mode is characterized by large, phased-aligned participation factors associated with all SM rotor speeds, indicating its system-wide nature. In this figure, a droop constant $R_{TG} = 0.05$ is used for all TGs. For the sake of comparison, Fig. 2b shows the participation factors for an electromechanical mode, which is local to the SM at bus 30. A time-domain simulation of the system further illustrates the behavior of the identified FR mode. We consider a three-phase fault at bus 6, occurring at $t = 1.0$ s and cleared after 80 ms by opening the line that connects buses 5 and 6. The response of the center-of-inertia (COI) frequency is shown in Fig. 3 and confirms the presence of a low-frequency oscillation around 0.01 Hz. As the droop constant R_{TG} is reduced the mode becomes faster, which is as expected.
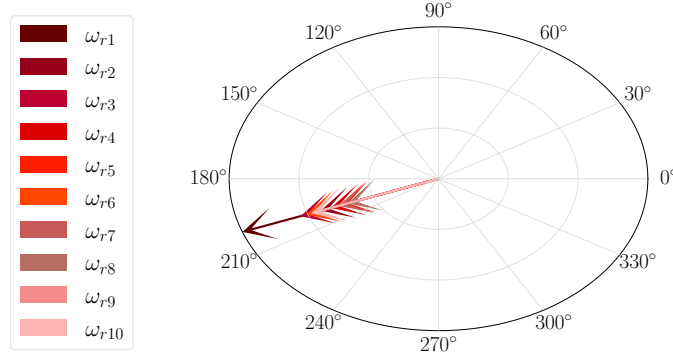
(a) Frequency regulation (FR) mode.
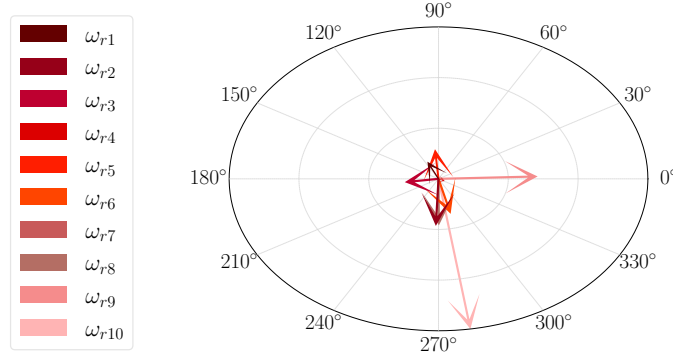
(b) Local electromechanical mode of SM at bus 30.

Figure 2: 39-bus system: SM rotor speed participation factors.

In the following, we employ the eigenvalue tracking method (19) to trace the FR mode under variations of key system parameters. We start by examining how the corresponding complex pair of eigenvalues evolves as the droop constant R_{TG} of the TGs is varied. Starting from an initial large value of $R_{TG} = 0.2$, the trajectory is tracked as the parameter decreases to 0.02. In Fig. 4, the results obtained via repeated QR factorizations serve as a reference. Performance of (19) is then illustrated for two numerical integration methods: forward Euler method (FEM) and 4-th order Runge-Kutta (RK4). Both methods accurately follow the mode trajectory when a sufficiently small parameter step is used. For the remainder of this case study, we use FEM due to its simplicity, although any standard integration method is applicable. Computational efficiency, which is of particular interest in large-scale systems, is discussed
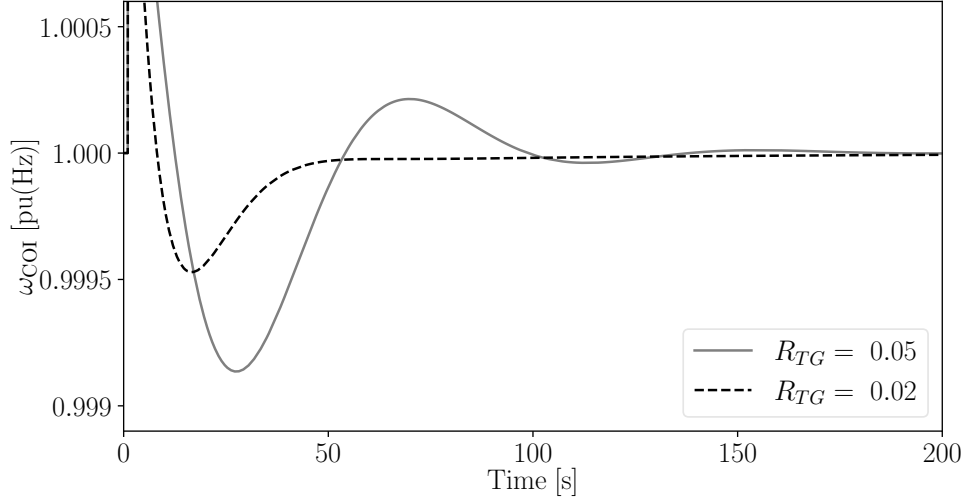
Figure 3: 39-bus system: Effect of TG droop on ω_{COI}.
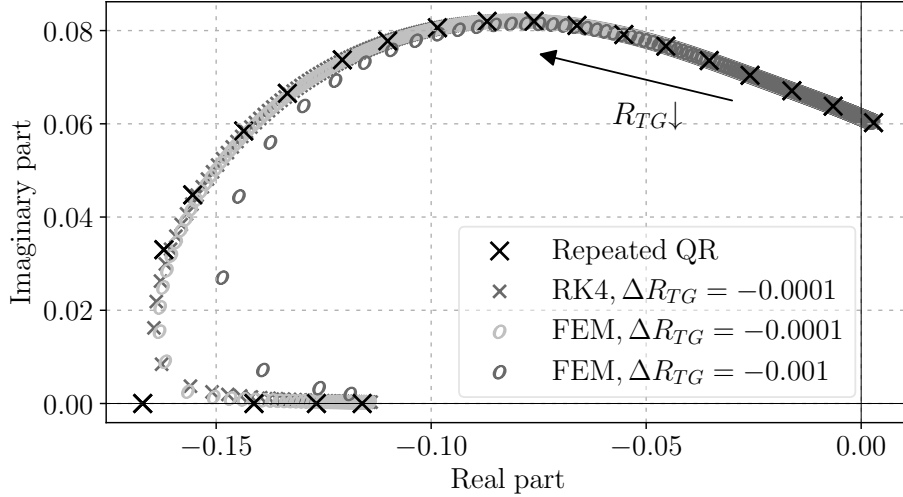
in Section 4.3.

Figure 4: 39-bus system, FR mode: Effect of varying $R_{TG} \in [0.01, 0.2]$.

Figure 4 is selected particularly because it showcases the behavior of (19) when it comes to capturing the trajectories of eigenvalues that go through a change of their spectral structure. Specifically, as R_{TG} decreases, a critical point is reached at which the complex pair of eigenvalues representing the FR mode becomes real. At this point, the eigenvalue becomes defective with algebraic multiplicity 2 and geometric multiplicity 1; that is, the system lacks a complete set of linearly independent eigenvectors as. This point corresponds to a *simple quadratic fold*. It occurs at a specific parameter value p for which the partial derivative $\partial s / \partial p$ of the traced eigenvalue does not exist, and the associated eigenvector becomes discontinuous [31].

As R_{TG} is further decreased, the defective eigenvalue in turn splits into two distinct real eigenvalues. Thereon, the tracking method inherently continues along one of the two resulting branches, determined by the numerical evolution of (19). In many cases, studying the second branch may not be of interest

11

as, at this point, both eigenvalues are perfectly damped. However, if the second branch is indeed of interest, we recommend that in practice the tracking process is reinitialized after the spectral splitting by recomputing an eigendecomposition of the system's pencil and extracting the eigenpair corresponding to that branch. The numerical and computational implications of this approach are further discussed later in this case study.

From Fig. 4, we also observe that a step size of $\Delta R_{TG} = -0.0001$ yields accurate tracking of the FR mode. Naturally, the choice of integration step size depends on the sensitivity of the eigenvalue to the parameter being varied. As an example, the same figure shows the impact of increasing the step size tenfold. Table 1 reports both the relative error in the eigenvalue and the error in its damping ratio for the two step sizes, highlighting the method's accuracy in capturing the mode's evolution. In practice, a key consideration for step-size selection is the Euclidean distance between the tracked eigenvalue at consecutive steps, i.e., between s_k and s_{k+1} computed via (19). This metric can also inform adaptive step-size control strategies, an aspect further discussed in Section 4.3.

Table 1: 39-bus system: Tracking accuracy as R_{TG} is varied.

| R_{TG} | $\Delta R_{TG} = 0.0001$ | | $\Delta R_{TG} = 0.001$ | |
	Relative error	$\Delta\zeta[\%]$	Relative error	$\Delta\zeta[\%]$
0.15	1.14×10^{-6}	0.00105	0.00011	0.00944
0.10	5.52×10^{-5}	0.00543	0.00055	0.04874
0.05	0.00034	0.02345	0.0034	0.21196
0.01	0.0046	0.00012	0.04875	0.01472

Figure 5 shows the performance of (19) when tracking the FR mode during a gradual decrease of up to 90% in the inertia constant M of the system's largest SM, which is connected to bus 39. This decrease in system inertia increases the speed of the FR mode. Notably, high tracking accuracy is maintained even for a large step of $\Delta M = -1$ pu [s].
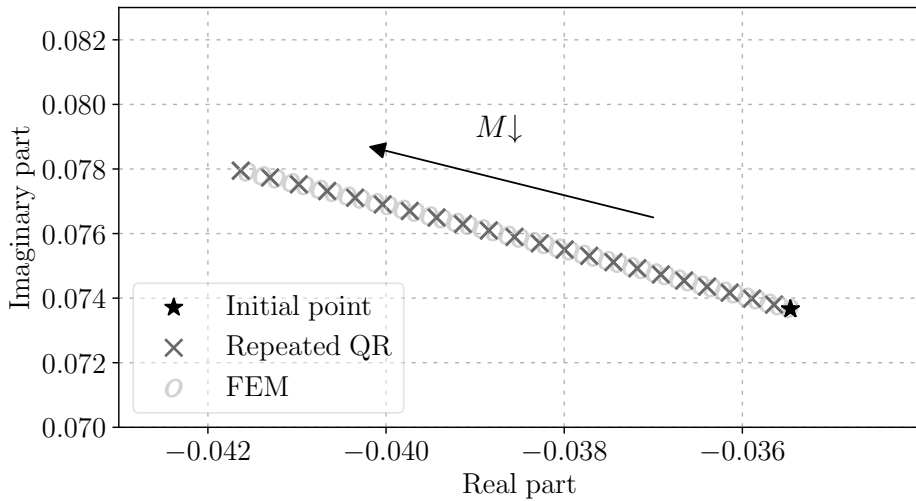

Figure 5: 39-bus system, FR mode: Effect of gradually reducing up to 90% the inertia of the SM at bus 39.

We next examine the accuracy of (19) under changes in the system's load model composition. Specifically, loads are modeled as a mix of constant power and constant impedance (Z) types. Starting from a system with all loads being constant power consumption, the share of constant impedance loads is gradually increased in 1% steps up to 100%. As shown in Fig. 6, with the increase of this share, the speed of the FR mode drops from 0.013 Hz to 0.005 Hz, while its damping reduces, specifically by 20%.
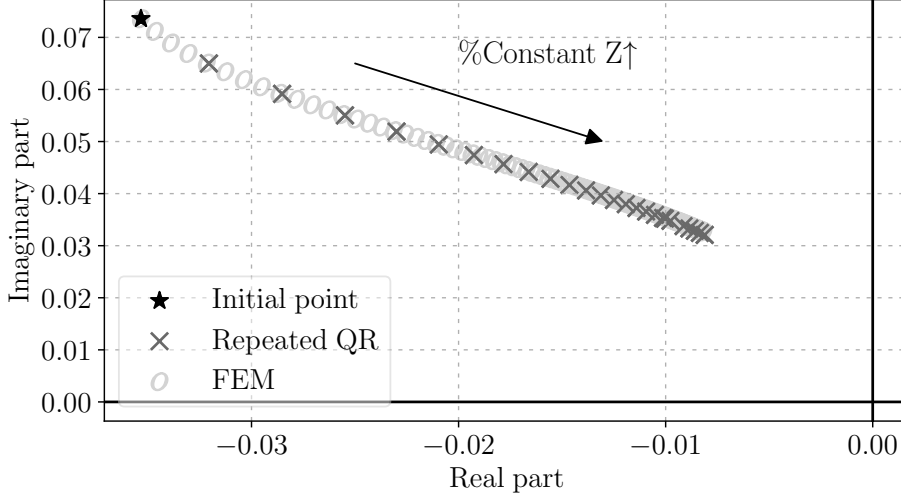

Figure 6: 39-bus system, FR mode: Effect of varying the share of constant impedance loads of the system from 0 to 100%.

4.2 Impact of Inverter-Based DERs

This section considers a modified version of the IEEE 39-bus system, in which half of the SMs are replaced by inverter-based distributed energy resources (DERs). Specifically, the SMs at buses 30, 34, 35, 36 and 37 are replaced by DERs of the same capacity. Each DER is represented by an inner control loop that regulates the d and q components of the current in the dq reference frame, along with two outer loops for primary frequency and voltage control [32]. The focus is again on tracking the FR mode via (19).

We start by gradually decreasing, from 0.2 to 0.01, the TG droop constants of the five remaining SMs. This variation leads to faster frequency control response and yields conclusions similar to those made for the original system. As shown in Fig. 7, decreasing R_{TG} results in a gradual increase of the FR mode's damping, reaching 100% at which point the complex pair of eigenvalues becomes real. Equation (19) can accurately track the eigenvalue of interest when the latter remains non-defective throughout the parameter variation. However, the transition from a complex-conjugate pair to two real eigenvalues passes through a defective eigenvalue. In this case, (19) inherently follows one of the resulting real eigenvalues, as shown in Fig. 7, where the imaginary part diminishes smoothly along the tracked trajectory.

When tracking is instead initialized from a real eigenvalue and the parameter is increased, the continuation-based formulation is unable to produce a complex pair at the point where the two real
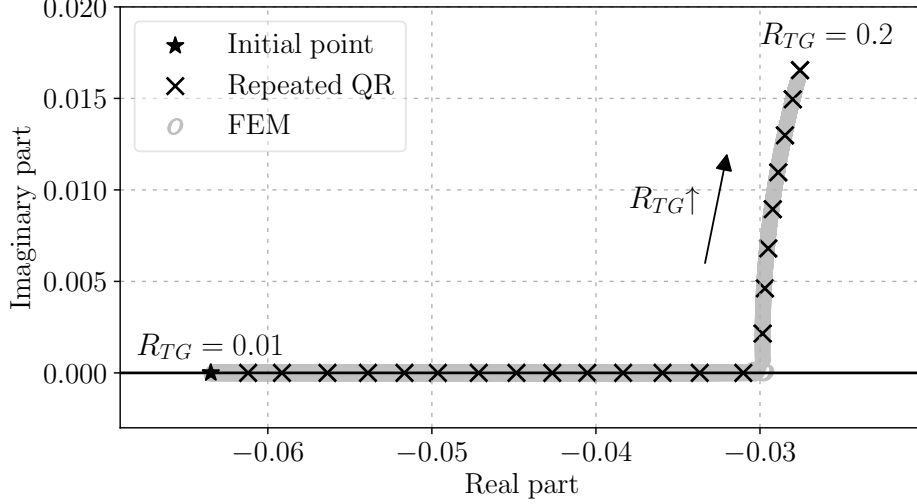
Figure 7: Modified 39-bus system, FR mode: Effect of varying TG droops in the range $[0.01, 0.2]$.

eigenvalues merge. To address this, a small imaginary part is introduced to the initial condition. Specifically, a term $j\epsilon$ is added to the initial eigenvalue $s_{\mathrm{i}}(p_{init})$ and to corresponding right eigenvector $\phi_{\mathrm{i}}(p_{init})$. In this way, the method can smoothly continue consistently through the transition and track the eigenvalue in the full range $R_{TG} \in [0.01, 0.2]$.

We next examine how the FR mode changes as the droop constants R_{DER} of the DER frequency controllers are varied. As shown in Fig. 8a, the eigenvalue associated with the FR mode moves progressively leftward in the complex plane as R_{DER} increases. Moreover, the damping ratio exhibits a non-monotonic trend: it decreases until reaching a minimum value of 87.35% at $R_{DER} = 0.027$, after which it begins to increase. This behavior is explained by considering the relative roles of DERs and SMs in frequency regulation. With the TG droop constants of SMs fixed at $R_{TG} = 0.05$, frequency regulation is initially dominated by the DERs. As R_{DER} increases, their frequency response weakens, and the SMs play an increasing role in shaping the mode's structure.

Varying the time constant T_f of the low-pass filter of the DER droop controllers has the opposite effect, as shown in Fig. 8b. As T_f increases, the controller response becomes slower, eventually suppressing the FR mode as the associated complex eigenvalues become real. The accuracy of (19) during this transition is summarized in Table 2.

Table 2: Modified 39-bus system: FR mode tracking as T_f varies.

T_f [s]	$\Delta T_f = 0.1$ s		$\Delta T_f = 1$ s	
	Relative error	$\Delta\zeta\%$	Relative error	$\Delta\zeta\%$
0.1	0	0	0	0
1	0.00007	0.00283	0.00229	0.02231
10	0.00059	0.02183	0.00573	0.22536
20	0.00105	0.02591	0.01001	0.26364
50	0.00649	−0.00123	0.06459	−0.20870
99	0.20693	−0.00002	0.20469	−0.00154

(a) Increasing the droop constant R_{DER} from 0.01 to 0.07.

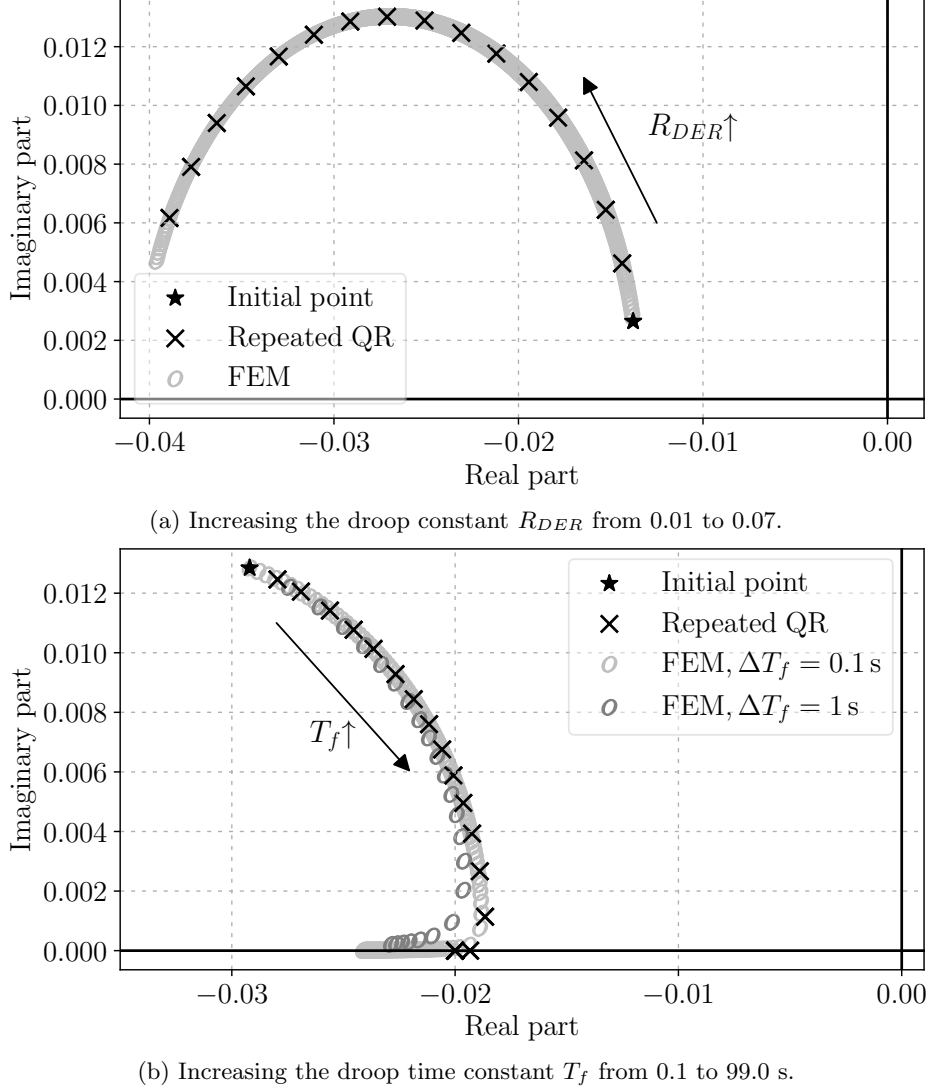(b) Increasing the droop time constant T_f from 0.1 to 99.0 s.

Figure 8: Modified 39-bus system, FR mode: Effect of varying the droop parameters of the DER frequency controllers.

Lastly, the effect of increasing the share of constant impedance loads is examined in Fig. 9. As this share increases, the damping of the FR mode decreases from 91.5% to 65.5%. Meanwhile, the mode's natural frequency reaches a maximum of 0.007 Hz when constant impedance loads are about 50% of the total.

4.3 All-Island Irish Transmission System

This section focuses on the computational efficiency of (19). To this end, we employ a larger system, namely a 1,502-bus dynamic model of the All-Island Irish Transmission System (AIITS). The model has in total $1,629$ states and $9,897$ algebraic variables. Such a size makes the use of dense QZ-based eigensolvers to handle the formulation in (5) impractical, with the resulting pencil having dimensions $11,526 \times 11,526$. In contrast, the state matrix associated with the dense formulation (7) is considerably smaller, at $1,629 \times 1,629$, and therefore provides a useful reference for benchmarking. Simulations in
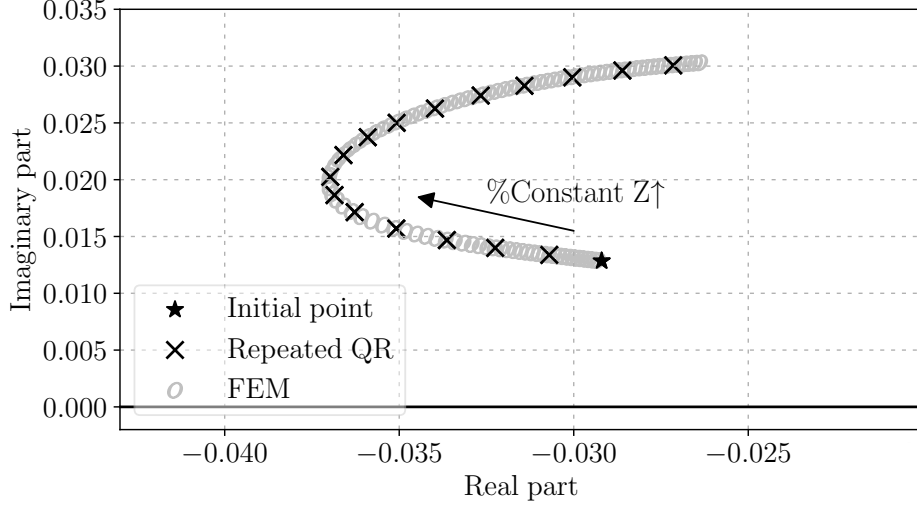
Figure 9: Modified 39-bus system, FR mode: Effect of varying the percentage of constant impedance loads from 0 to 100%.

this section are executed using a computer with a 13th Gen Intel Core i7-13700, 2.10 GHz processor, 16 GB of RAM, and running a 64-bit Linux OS.
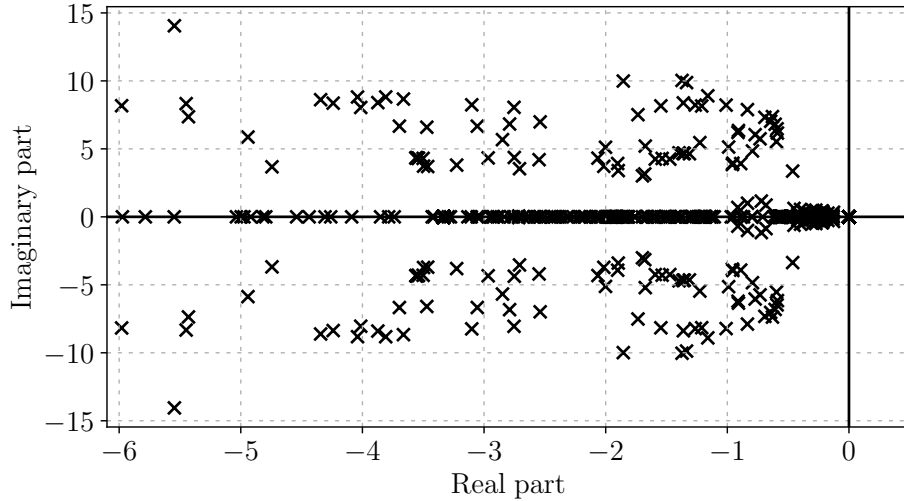

Figure 10: AIITS root locus.

As shown in the root locus of Fig. 10, the high density of eigenvalues in the complex plane highlights that tracking a specific mode of interest can become a challenging task. Firstly, we consider the formulation in (5) – which results in a $11,526 \times 11,526$ system problem – and focus on the region of the complex plane where poorly damped electromechanical modes are located. We gradually increase the gains K_w of the 6 power system stabilizers (PSSs) of the AIITS model from 1.5 to 9.5, and we sequentially trace a group of modes, shown in Fig. 11. The results confirm that (19) captures the eigenvalue trajectories with high precision.

Unlike approaches that rely solely on Newton's method to compute eigenvalues at each parameter step (e.g., [11]), the approach adopted in this paper is based on continuous integration and can, if needed,
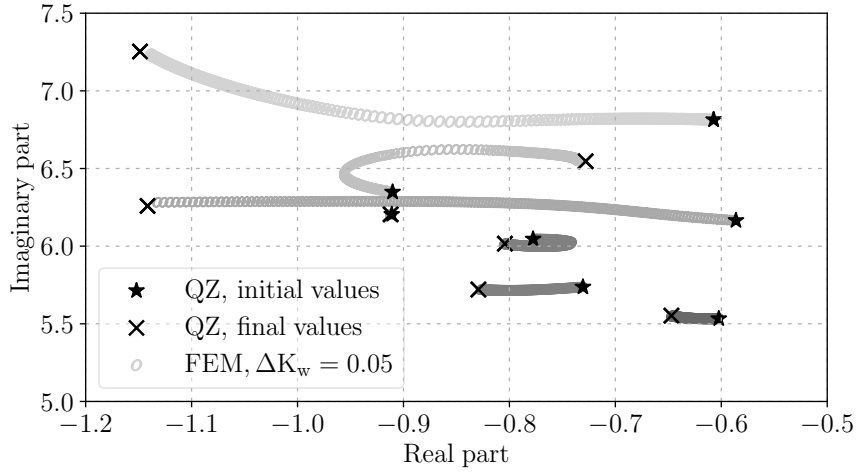
16

Figure 11: AIITS: Poorly damped electromechanical modes when the gains of the PSSs are varied.

be combined with a Newton corrector to further improve accuracy. This reduces the risk of divergence or convergence to incorrect values, particularly when large steps need to be used to boost computational efficiency. As shown in Fig. 12, using a large step to track one of the system's electromechanical modes over the interval $K_w = [1.5, 41.5]$ causes Newton's method, when applied directly to the eigenvalue problem, to deviate from the correct trajectory. In contrast, (19) combined with a Newton corrector step consistently follows the correct eigenvalue trajectory, benefiting from more accurate intermediate estimates and improved convergence.
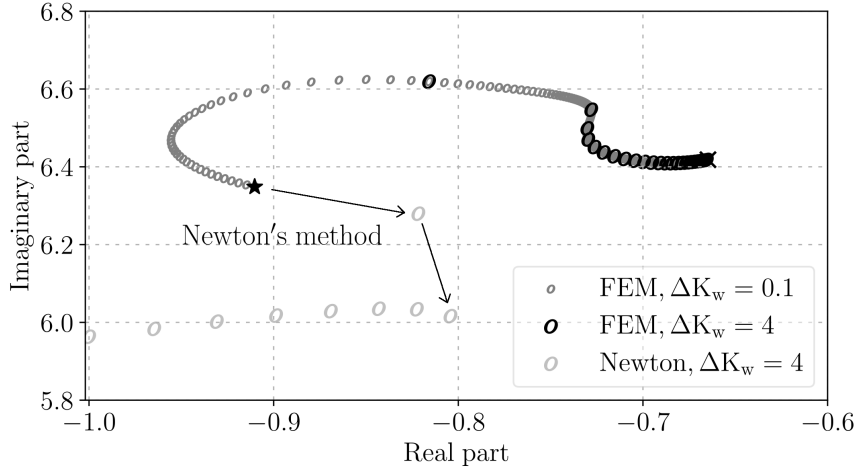

Figure 12: AIITS: Tracking an electromechanical mode: Newton vs integration-based continuation.

Subsequently, we employ the formulation in (7). A poorly damped mode of the system (initially located at $-0.71087 \pm j1.16143$) is tracked as the TG droop constants of all SMs are gradually increased from 0.02 to 0.2. The results for two different values of ΔR_{TG} are shown in Fig. 13. As summarized in Table 3, (19) is able to track the mode with high accuracy. In terms of computational efficiency, the

benchmark considered is the total time required to trace an eigenvalue over the range $[0.02, 0.2]$ using a step size of $\Delta R_{TG} = 0.0025$. As shown in Table 4, (19) achieves a tenfold reduction of computation time compared to repeated QR factorizations. The average time recorded for solving the power flow problem is 0.05 s, with an additional 0.016 s spent on post-processing tasks, including the construction of system matrices. Therefore, the steady-state analysis step incurs an average overhead of 0.066 s per iteration.
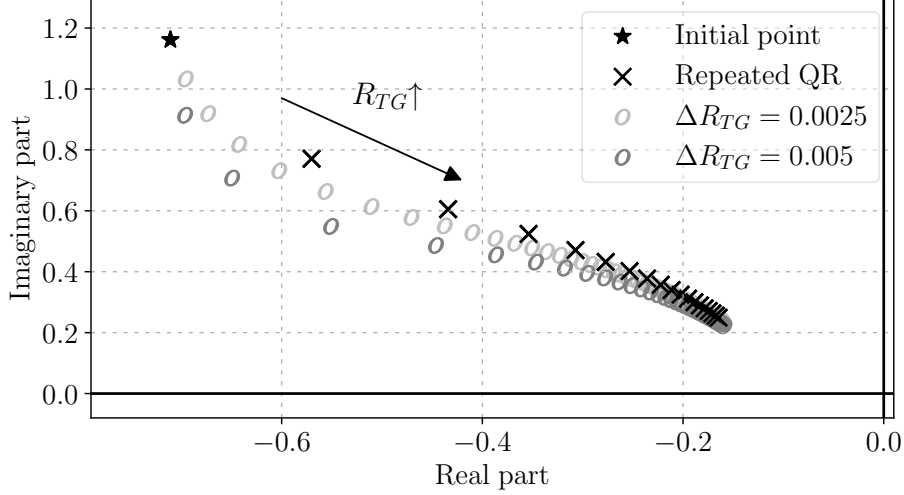

Figure 13: AIITS: Tracking of an electromechanical mode when the droop constant R_{TG} of all SMs is varied.

Table 3: AIITS: Tracking accuracy for R_{TG} variation.

| R_{TG} | $\Delta R_{TG} = 0.0025$ | | $\Delta R_{TG} = 0.005$ | |
	Relative error	$\Delta\zeta\%$	Relative error	$\Delta\zeta\%$
0.02	0	0	0	0
0.05	0.07146	3.07406	0.14665	6.65217
0.075	0.06434	1.80305	0.12820	4.22215
0.1	0.05955	1.58114	0.11782	3.67346
0.15	0.05233	1.38234	0.10325	3.22334
0.2	0.04665	1.29035	0.09214	2.99423

Table 4: AIITS: Tracking computational cost comparison.

	Total time	After initial QR	1-step
Repeated QR	459.54 s	453.67 s	6.30 s
Eq. (19)	47.58 s	41.39 s	0.57 s

To further improve efficiency, we implement a simple adaptive step size strategy, where the integration step ΔR_{TG} is doubled or halved based on the Euclidean distance $|\Delta s|$ between two successive values of the tracked eigenvalue. Specifically, the step is doubled if $|\Delta s| < 0.04$ and halved if $|\Delta s| > 0.08$. Figure 14 shows the result of applying this adaptive strategy, starting from an initial step size of 0.0025. The total computation time is significantly reduced from 47.58 s (constant step) to 18.28 s. As seen by comparing Figs. 13 and 14, this efficiency gain comes at a negligible cost in accuracy.
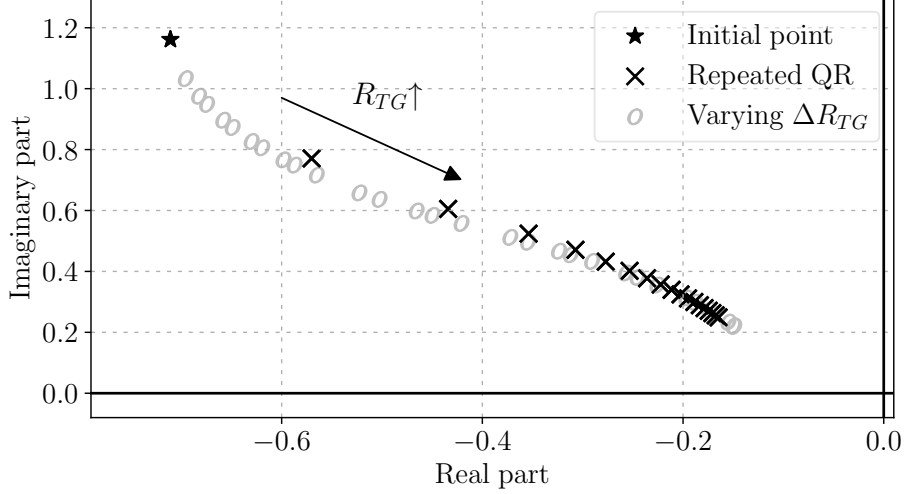
Figure 14: AIITS: Poorly damped mode tracking as R_{TG} is varied.

5 Conclusion

This paper focuses on continuation-based eigenvalue tracking of large-scale power system models. A general formulation is presented that supports both dense and sparse matrix representations and enables efficient integration-based tracking of targeted eigenvalues. Key implementation aspects are discussed in detail. The approach is first evaluated through a case study targeting the frequency regulation mode under various parameter variations. Computational efficiency and scalability are then discussed based on a 1,502-bus model of the Irish transmission system. Future work will explore extensions to more general classes of models, such as systems affected by measurement and communication delays.

6 Funding

Appendix A   Derivation of (17)

The derivation of (17) goes as follows. Differentiation of (16) with respect to $p \in \mathbb{R}$ gives:

$$\dot{\boldsymbol{\phi}}^{\mathsf{T}}\mathbf{E}\boldsymbol{\phi} + \boldsymbol{\phi}^{\mathsf{T}}\mathbf{E}\dot{\boldsymbol{\phi}} = -\boldsymbol{\phi}^{\mathsf{T}}\dot{\mathbf{E}}\boldsymbol{\phi}. \tag{A.1}$$

Let us denote as ϕ_i the i-th element of $\boldsymbol{\phi}$ and as e_{ij} the element of the i-th row and j-th column of $\mathbf{E}$. By rewriting $\dot{\boldsymbol{\phi}}^{\mathsf{T}}\mathbf{E}\boldsymbol{\phi}$ as a sum, it is straightforward that:

$$
\begin{aligned}
\dot{\boldsymbol{\phi}}^{\mathsf{T}}\mathbf{E}\boldsymbol{\phi} &= \sum_{k=1}^{r}\sum_{l=1}^{r}\dot{\phi}_l e_{kl}\phi_l \\
&= \sum_{k=1}^{r}\sum_{l=1}^{r}\phi_l e_{kl}\dot{\phi}_l = \boldsymbol{\phi}^{\mathsf{T}}\mathbf{E}\dot{\boldsymbol{\phi}}.
\end{aligned}
\tag{A.2}
$$

Combining (A.2) and leads to (17).

References

[1] F. Milano, I. Dassios, M. Liu, and G. Tzounas, *Eigenvalue Problems in Power Systems*. CRC Press, 2020.

[2] C. Tajoli, G. Tzounas, and G. Hug, "Mode-shape deformation of power system DAEs by time-domain integration methods," in *2023 IEEE Belgrade PowerTech*. IEEE, 2023, pp. 1–6.

[3] M. Pastor, M. Binda, and T. Harčarik, "Modal assurance criterion," *Procedia Engineering*, vol. 48, pp. 543–548, 2012.

[4] G. Tzounas, I. Dassios, M. Liu, and F. Milano, "Comparison of numerical methods and open-source libraries for eigenvalue analysis of large-scale power systems," *Applied Sciences*, vol. 10, no. 21, p. 7592, 2020.

[5] R. B. Lehoucq and D. C. Sorensen, "Deflation techniques for an implicitly restarted Arnoldi iteration," *SIAM Journal on Matrix Analysis and Applications*, vol. 17, no. 4, pp. 789–821, 1996.

[6] G. W. Stewart, "A Krylov–Schur algorithm for large eigenproblems," *SIAM Journal on Matrix Analysis and Applications*, vol. 23, no. 3, pp. 601–614, 2002.

[7] T. Sakurai and H. Sugiura, "A projection method for generalized eigenvalue problems using numerical integration," *Journal of computational and applied mathematics*, vol. 159, no. 1, pp. 119–128, 2003.

[8] V. Ajjarapu and C. Christy, "The continuation power flow: a tool for steady state voltage stability analysis," *IEEE Transactions on Power Systems*, vol. 7, no. 1, pp. 416–423, 1992.

[9] C. A. Canizares and F. L. Alvarado, "Point of collapse and continuation methods for large AC/DC systems," *IEEE Transactions on Power Systems*, vol. 8, no. 1, pp. 1–8, 1993.

[10] X. Wen and V. Ajjarapu, "Application of a novel eigenvalue trajectory tracing method to identify both oscillatory stability margin and damping margin," *IEEE Transactions on Power Systems*, vol. 21, no. 2, pp. 817–824, 2006.

[11] C. Li, G. Li, C. Wang, and Z. Du, "Eigenvalue sensitivity and eigenvalue tracing of power systems with inclusion of time delays," *IEEE Transactions on Power Systems*, vol. 33, no. 4, pp. 3711–3719, 2017.

[12] C. Luo and V. Ajjarapu, "Sensitivity-based efficient identification of oscillatory stability margin and damping margin using continuation of invariant subspaces," *IEEE Transactions on Power Systems*, vol. 26, no. 3, pp. 1484–1492, 2011.

[13] Q. Mou, Y. Xu, H. Ye, and Y. Liu, "An efficient eigenvalue tracking method for time-delayed power systems based on continuation of invariant subspaces," *IEEE Transactions on Power Systems*, vol. 36, no. 4, pp. 3176–3188, 2021.

[14] Z. Zeng, "Sensitivity and computation of a defective eigenvalue," *SIAM Journal on Matrix Analysis and Applications*, vol. 37, no. 2, pp. 798–817, 2016.

[15] I. Dobson, J. Zhang, S. Greene, H. Engdahl, and P. W. Sauer, "Is strong modal resonance a precursor to power system oscillations?" *IEEE Transactions on Circuits and Systems I: Fundamental Theory and Applications*, vol. 48, no. 3, pp. 340–349, 2001.

[16] D. Wang, L. Liang, L. Shi, J. Hu, and Y. Hou, "Analysis of modal resonance between pll and dc-link voltage control in weak-grid tied vscs," *IEEE Transactions on Power Systems*, vol. 34, no. 2, pp. 1127–1138, 2018.

[17] F. Milano, "Semi-implicit formulation of differential-algebraic equations for transient stability analysis," *IEEE Transactions on Power Systems*, vol. 31, no. 6, pp. 4534–4543, Nov. 2016.

[18] F. Milano, M. Liu, M. A. Murad, G. M. Jónsdóttir, G. Tzounas, M. Adeen, Á. Ortega, and I. Dassios, "Power system modelling as stochastic functional hybrid differential-algebraic equations," *IET Smart Grid*, vol. 5, no. 5, pp. 309–331, 2022.

[19] P. Kundur, *Power System Stability and Control*. New York: Mc-Grall Hill, 1994.

[20] I. Dassios, G. Tzounas, and F. Milano, " The Möbius transform effect in singular systems of differential equations," *Applied Mathematics and Computation*, vol. 361, pp. 338–353, 2019.

[21] I. Dassios, G. Tzounas, and F. Milano, "Robust stability criterion for perturbed singular systems of linearized differential equations," *Journal of Computational and Applied Mathematics*, vol. 381, p. 113032, 2021.

[22] A. Bouhamidi and K. Jbilou, "A note on the numerical approximate solutions for generalized Sylvester matrix equations with applications," *Applied Mathematics and Computation*, vol. 206, no. 2, pp. 687–694, 2008.

[23] B. Zhou and G.-R. Duan, "On the generalized Sylvester mapping and matrix equations," *Systems & Control Letters*, vol. 57, no. 3, pp. 200–208, 2008.

[24] L. Jin, J. Yan, X. Du, X. Xiao, and D. Fu, "RNN for solving time-variant generalized Sylvester equation with applications to robots and acoustic source localization," *IEEE Transactions on Industrial Informatics*, vol. 16, no. 10, pp. 6359–6369, 2020.

[25] V. Simoncini, "Computational methods for linear matrix equations," *SIAM Review*, vol. 58, no. 3, pp. 377–441, 2016.

[26] Illinois Center for a Smarter Electric Grid (ICSEG), "IEEE 39-Bus System," publish.illinois.edu/smartergrid/ieee-39-bus-system/.

[27] F. Milano, "A Python-based software tool for power system analysis," in *Proceedings of the IEEE PES General Meeting*, Jul. 2013.

[28] F. Wilches-Bernal, J. H. Chow, and J. J. Sanchez-Gasca, "A fundamental study of applying wind turbines for power system frequency control," *IEEE Transactions on Power Systems*, vol. 31, no. 2, pp. 1496–1505, 2016.

[29] A. Moeini and I. Kamwa, "Analytical concepts for reactive power based primary frequency control in power systems," *IEEE Transactions on Power Systems*, vol. 31, no. 6, pp. 4217–4230, 2016.

[30] F. Milano, B. Alhanjari, and G. Tzounas, "Enhancing frequency control through rate of change of voltage feedback," *IEEE Transactions on Power Systems*, vol. 39, no. 1, pp. 2385–2388, 2023.

[31] J. Sun, "Multiple eigenvalue sensitivity analysis," *Linear algebra and its applications*, vol. 137, pp. 183–211, 1990.

[32] Álvaro Ortega and F. Milano, "Frequency control of distributed energy resources in distribution networks," *IFAC-PapersOnLine*, vol. 51, no. 28, pp. 37–42, 2018.